Computational histology reveals that concomitant application of insect repellent with sunscreen impairs UV protection in an ex vivo human skin model

Sophie Charrasse, Titouan Poquillon, Charlotte Saint-Omer, Audrey Schunemann, Mylène Weill, Victor Racine, Abdel Aouacheria

Parasites & Vectors

RESEARCH

Open Access

Computational histology reveals that concomitant application of insect repellent with sunscreen impairs UV protection in an ex vivo human skin model

Sophie Charrasse[1], Titouan Poquillon[1,2], Charlotte Saint-Omer[1], Audrey Schunemann[3], Mylène Weill[1], Victor Racine[2] and Abdel Aouacheria[1*]

Abstract

Background Histological alterations such as nuclear abnormalities are sensitive biomarkers associated with diseases, tissue injury and environmental insults. While visual inspection and human interpretation of histology images are useful for initial characterization, such low-throughput procedures suffer from inherent limitations in terms of reliability, objectivity and reproducibility. Artificial intelligence and digital morphometry offer unprecedented opportunities to quickly and accurately assess nuclear morphotypes in relation to tissue damage including skin injury.

Methods In this work, we designed NoxiScore, a pipeline providing an integrated, deep learning-based software solution for fully automated and quantitative analysis of nucleus-related features in histological sections of human skin biopsies. We used this pipeline to evaluate the efficacy and safety of three dermato-cosmetic products massively sold at the time of the study in the Montpellier area (South of France): a sunscreen containing UV filters, a mosquito repellent (with synthetic active ingredient IR3535) and a product combining a natural insect repellent plus a sunscreen. Hematoxylin and eosin or hematoxylin-eosin saffron staining was performed to assess skin structure before morphometric parameter computation.

Results We report the identification of a specific nuclear feature based on variation in texture information that can be used to assess skin tissue damage after oxidative stress or UV exposure. Our data show that application of the commercial sun cream provided efficient protection against UV effects in our ex vivo skin model, whereas application of the mosquito repellent as a single product exerted no protective or toxic effect. Notably, we found that concurrent application of the insect repellent with the sunscreen significantly decreased the UVB protective effect of the sunscreen. Last, histometric analysis of human skin biopsies from multiple donors indicates that the sunscreen-insect repellent combo displayed variable levels of protection against UV irradiation.

Conclusions To our knowledge, our study is the first to evaluate the potential toxicity of combining real-life sunscreen and insect repellent products using ex vivo human skin samples, which most closely imitate the cutaneous physiology. The NoxiScore wet-plus-dry methodology has the potential to provide information about the pharmaco-toxicological profile of topically applied formulations and may also be useful for diagnostic purposes and evaluation of the skin exposome including pesticide exposure, air pollution and water contaminants.

*Correspondence:
Abdel Aouacheria
abdel.aouacheria@umontpellier.fr
Full list of author information is available at the end of the article

Keywords Insect repellent, Organelle biology, Image analysis, Sunscreen, Morphometry, Histology, Exposome, Toxicology

Background

Skin is the largest organ in the body and covers its entire external surface, acting as a biological barrier. Evolution of human skin barrier is characterized by specific genetic changes that have occurred since humans diverged from their ancestors [1] and thereafter into separate populations [2]. On a daily basis, this skin barrier is the first line of defense against physical environmental stressors [like ultraviolet (UV) radiation, blue light, high temperatures and mechanical injury], biological hazards (from bacteria, viruses, fungi, insect bites and allergens) and a wide range of environmental chemicals (including particulate matter, persistent organic pollutants, tobacco smoke, pesticides, heavy metals, etc.) [3–5].

Exposure of the human skin to foreign substances may be incidental (i.e. environmental) but can also be deliberate, such as the use of cosmetic products and pharmaceuticals. In this respect, improved awareness of skin cancers and vector-borne diseases has led to a rise in the use of sunscreens and insect repellents, especially during the summer months. Indeed, public concerns about Zika, malaria, dengue, chikungunya and West Nile virus (which are transmitted by mosquitoes), as well as Lyme borreliosis (which is spread to humans by infected ticks), have increased requests for individual protection solutions against arthropod bites [6, 7]. The World Health Organization (WHO) recommends using insect repellents as a gold standard for protection against arthropods and their associated diseases [8]. Repellents are not meant to kill insects but to keep them away to prevent bites and the spread of diseases. Insect repellent formulations can be purchased as lotions, pump sprays, aerosols or impregnated material (such as wet wipes and roll-ons). While synthetic molecules like N, N-diethyl-m-toluamide (DEET), 3-[N–n-butyl-N-acetyl] aminopropionic acid ethylester (also known as Insect Repellent 3535 or IR3535), picaridin, permethrin and N,N-diethyl phenylacetamide (DEPA) are primary ingredients in commercially available formulations [9–11], repellents of natural origin have also entered the market [such as para-menthane-3,8-diol (PMD), eucalyptus and citronella oils and other plant-derived ingredients] [12, 13]. Recently, there has been a growing demand for insect repellent products as more people are engaging in outdoor activities [14], with several mosquito species (like *Aedes albopictus*) feeding during the day. Recreational UV exposure has also dramatically increased in recent years because of outdoor activities and skin tanning for aesthetic purposes [15, 16]. Because solar UV rays are well known to cause cutaneous cancers and premature skin aging (characterized by wrinkles, loss of skin elasticity and age dyschromia) [17], health authorities recommend using sunscreens to prevent photoallergic reactions. Sunscreen formulations are generally available in lotions, gels, sprays, aerosols, suntan oils and sticks that should be applied generously to cover all exposed skin [18]. Such recent tendencies have contributed to the increase in application of sunscreens and insect repellents, both separately and combined within a single product. With climate change bringing warmer temperatures and insect outbreaks (such as in the Languedoc coast and Camargue, two areas in southern France), it is anticipated that people will increasingly incorporate these products into their daily routines.

Establishing recommendations for proper use of sunscreens and insect repellents, both separately and concurrently, is challenging [19–23] because of the wide spectrum of commercial preparations and the difficulty of finding a balance between applying effective products (i.e. products offering the greatest protection in real-life conditions of temperature, humidity, sweat and abrasion) and limiting their potential for skin irritation, dermal toxicity and systemic adverse responses. For decades, animal-based test procedures for evaluating skin and ocular irritation (such as the rabbit Draize test) were considered the gold standard for risk assessment of consumer products. However, such highly invasive tests have been criticized because of concerns about animal welfare and unnecessary use of animals and for their limited transferability to the human organism because of interspecies differences. This led to several legislative changes and implementation of alternative, animal-free toxicity testing methods [24–26]. The use of in vitro human skin models offers an interesting alternative to animal testing for the evaluation of dermato-cosmetic products like insect repellents and sunscreens [27]. While skin cell cultures and in vitro-reconstructed models may be useful for initial product testing [28–30], such systems suffer from inherent limitations in terms of cell population, viability, structure and function (including metabolism, immunity and cutaneous barrier properties) as they are not exact copies of the human skin. In contrast, ex vivo skin explants (skin biopsies) contain the full architecture of the human skin (including the

epidermis, dermis, skin appendages and immune cells) and have thus emerged as a model of choice to evaluate skin toxicity and pharmacology in vitro [31–34]. In this system, tissue viability and integrity can be assessed indirectly [e.g. through the methyl thiazolyl tetrazolium (MTT) assay] or directly through histological analysis after hematoxylin and eosin (HE) staining of skin tissue explant sections [35].

The advent of computational image analysis techniques has raised the possibility that objective quantification of staining properties will gain importance in providing data for toxicological or diagnostic purposes. For instance, we recently developed a series of quantitative imaging tools to measure changes in mitochondrial morphology in stressed vs. control cells [36–38]. Likewise, any given cell type has an associated "normal" nuclear morphology. Here, we reasoned that deviations of nuclear shape can indicate tissue injury due to toxic damage to cells in the same way that nuclear abnormalities characterize certain types of diseases, such as cancer [39–46], Emery-Dreifuss muscular dystrophy [47–49], premature aging disorders like progeria syndromes [50, 51], trisomy 21 [52] and tauopathies [53]. To accurately assess nuclear and nucleus-associated spatial abnormalities, it is important to use quantitative measures of nuclear morphology instead of visual inspection and to take advantage of the new opportunities offered by artificial intelligence (AI). In this work, we developed a novel software (named NoxiScore) that uses deep learning techniques to detect nuclei in histological images of skin samples. We report the identification of a specific feature based on variation in nuclear morphometric information that can be used to assess skin tissue damage after oxidative stress, UV exposure and/or treatment with dermato-cosmetic products. Based on this novel indicator, our results indicate that, when administered concurrently, a widely used mosquito repellent can mitigate the protective effects on skin explants of a popular sun cream despite its high SPF (Sunburn Protection Factor) value.

Methods

Skin explant model

NativeSkin® 8-mm-diameter live human skin explants (normal human skin biopsies) were purchased from Genoskin SAS (Toulouse, France). These human skin models were collected from healthy donors who underwent abdominoplasty procedures and had given informed consent. This biological material is in full compliance with the Declaration of Helsinki and all other applicable regulations. The present study is not classified as human subject research, and no Institutional Review Board approval was required. For each donor, 10 to 12 samples were generated from skin unexposed to solar radiation (with a total number of 4 donors). The NativeSkin kit, containing 12-well plates loaded with round skin biopsies and recommended culture medium, was used according to the manufacturer's instructions. Each sample showed normal morphology and preserved skin structure, as attested by the internal quality check (histological validation) carried out by the manufacturer prior to shipping. The skin biopsies were reported lesion-free, histologically validated and virologically negative for HIV-1 and -2, hepatitis B and C and SARS-CoV-2 (see Additional file 1 for information related to skin type). NativeSkin samples can be cultured ex vivo up to 7 days at 37 °C with 5% CO_2 and maximal humidity, without loss of tissue integrity, viability and barrier properties [54, 55]. After their delivery, the skin explants were refreshed with new medium and kept in culture prior to treatment. The culture medium was renewed every day.

Products

Product selection was made based on a local market survey of the best-selling sunscreens, insect repellents and "combos" available for commercial distribution in the area of Montpellier (South of France). A list of items was prepared from local retail stores, including local pharmacies, supermarkets, outdoor gear shops, department stores, convenience stores and cosmetics stores. Non-topical mosquito repellent products, including those in the form of wristbands and patches, those used on clothing and outdoor gear, and area repellents such as lanterns and coils, were excluded. The survey was conducted between April 3–7, 2022. The items chosen for experimental analysis were the mosquito repellent with the commercial name "Cinq sur Cinq TROPIC 353D06-04.21" (containing IR3535 at the concentration of 35% w/w), the sunscreen "Nivea Sun sensitive "protection immediate 50+" (containing the UV filters butyl methoxydibenzoylmethane, ethylhexyl triazone, bis-ethylhexyloxyphenol methoxyphenyl triazine) and the combo "Cinq sur Cinq Spray Citriodora FPS50" (containing the same UV filters plus plant-based extracts including *Eucalyptus citriodora* oil (hydrated, cyclized) (CAS 1245629-80-4; 10 g/100 g)). Full ingredient lists of the formulations are available as Additional file 2. The items were purchased at a local hypermarket. All the products passed full safety testing before reaching the market and were thus not assayed here for their toxicity.

Treatments

Skin explant samples (8 mm diameter, ~ 50 mm^2) were dried by removing the culture medium and rapidly patting them with a sterilized pad. The tested products were applied to the skin explants, and the multi-well plates were then refilled with fresh media. When applied separately as individual substances, 50 µl insect repellent or sunscreen (corresponding to ~ 0.13–0.15 mg/cm^2) was

applied to each NativeSkin sample for 30 min. In combined application, 25 µl of each substance was layered, with the sunscreen first and then the insect repellent (as recommended by the Centers for Disease Control and Prevention) [56, 57]. Dulbecco's phosphate-buffered saline (from Gibco) was used as a negative control and treatment with 3% H_2O_2 (Sigma) for 24 h as a positive control of tissue damage. Protocol for H_20_2 administration was adapted from [58] (see 'Systemic administration'). For experiments involving controlled UVB irradiation, 12-well plates loaded with NativeSkin explants were placed within a BS-02 UV irradiation chamber equipped with UV-Mat dosimeter (Dr. Gröbel UV-Elektronik GmbH, Ettlingen, Germany) as previously described [36, 38]. The lamp emits UVB with a peak at 311–312 nm and partially excludes shorter wavelengths, such as UVA. Skin explants were maintained in their nourishing matrix during the irradiation process at the dose of 300 mJ/cm^2 (irradiation time of ~ 3 min and irradiation area of the chamber being 40 × 29 cm), and fresh culture medium was added immediately after UVB exposure. To detect macroscopic defects on tissue structural integrity, post-treatment incubation duration was set at 24 h or 48 h, the classical timepoints used in similar experimental settings [59–62]. The products were also tested in conditions of exposure to real sunlight. Briefly, skin biopsies underwent one outdoor sun exposure to a high UV index (of 8) for 2 h (corresponding to ~ 144 mJ/cm^2). The UV index was collected from Meteo France (Montpellier city, France; June 13, 2022, from 1 to 3 p.m.). Of the two skin explants that had no sunscreen or mosquito repellent, one was exposed to sunlight for 2 h (untreated skin, positive control for solar UV-induced skin damage) and one was not exposed at all (unexposed skin, i.e. negative control for solar UV-induced skin damage). Note that the single and layered products were not removed throughout the experiments.

Histological preparation and slide scanning

At the end of the post-treatment incubation period (24 to 48 h), biopsies were fixed in 10% neutral-buffered formalin for 48 h and stored in 70% ethanol before inclusion in paraffin and slicing (at RHEM platform, Biocampus, Montpellier, France). In a first set of experiments (12 separate conditions), 42 cross-sections from a single epidermis of 3 µm thickness (10 µm apart) were prepared using a Microm HM355-S semiautomatic microtome (Thermo Scientific). In a second set of experiments (14 separate conditions), 18 cross-sections were prepared from three different donors. Hematoxylin and eosin (HE) or hematoxylin-eosin-saffron (HES) staining was performed to assess skin structure. In HE, hematoxylin stains nucleic acids, whereas eosin counter-staining is used to detect the cytoplasmic proteins. In HES, saffron highlights the dermis (by staining collagen yellow). Images were taken by the slide scanning system Hamamatsu NanoZoomer® 2.0 HT (with × 40 objective, 0.23 µm/pixel, giving 180,000*90,000 pixels, 24-bit color image NDPI files), and the virtual slide system Hamamatsu NDP.view was used to observe and measure sections (MRI-INM, Montpellier, France). All slides were scanned at 20× magnification.

Software implementation

We used the software application HistoMetriX(M) (QuantaCell, France), a computer vision solution dedicated to histology analysis coupled to a deep learning framework. A graphical user interface allows users to upload their images, assess parameters, select a quantification procedure, launch batch processing on all slides of the project and view the results. The output is made of all the segmentation masks (nuclei, cells and epidermis) and a.csv file with all the quantitative results associated with the nuclei detected in a given epidermis. The user can choose to test different analysis steps on a defined area within the image before full image quantification on the entire image. To handle the large size of images, results (masks, assemblies) were exported into a pyramidal image format using the DZI standard [63].

AI-assisted morphometric image analysis

An automatic ROI detection algorithm is first applied to detect only the skin areas and remove the background parts of the image. The second step involves the detection of epidermis and nuclei using pretrained CNN (U-Net [64] and StarDist, [65] networks, respectively). Calibration of segmentation parameters is performed using the previsualization tool (two left images). Then, the entire set of digitized images is processed automatically on a tiled image, allowing for AI use on very large samples and at high resolution. The quantification of nuclear parameters is then performed, initially on tiled images and then merged tiles for optimal computational efficiency. The measured descriptors can be previewed before full processing in order to focus on descriptors of interest. It is possible to extract shape information (area, perimeter, aspect ratio, etc.), intensity information (mean values, variance, extreme values), texture information (GLCM contrast, GLCM energy, GLCM entropy [66]) and density information (number of neighbors, distance to the nearest neighbor) as well as, for the nuclei, their location within the epidermis. All results are then exported in.csv format. Each tile (1024 × 1024 pixels at a resolution of 20x) classically contains around 7000 nuclei. Each tissue sample takes approximately 4 min to analyze.

NoxiScore application

NoxiScore application is a homemade application developed in Python using a graphical interface made in QT, and statistical toolboxes allow performing statistical analyses applied to different groups of tissue samples. This module loads mask results and features associated to individual detected objects (nuclei, epidermis).

Statistics

Statistical analysis includes different statistical tools including t-test, PCA, LDA, SSMD and many data representations (charts, radars, histograms) adapted to sample analysis. This interface allows the user to define the different conditions of the samples and perform group comparisons, measurements and visualization of the effects of treatments. In the presented results, values for each descriptor are compared by the paired t-test. Significance was set as $P<0.05$. These are tests of significance between two conditions/groups; first, an untreated skin sample is compared with a sample subjected to solar or UVB stress. Then, each sample, pretreated with a product (sunscreen and/or insect repellent), is compared with the sample subjected to UV stress. The difference between the means of the two groups analyzed is plotted on a histogram. Total number of analyzed nuclei is given in legends to Figs. 3 and 4 and Additional file 4.

Data storage and availability

The datasets used and/or analyzed during the current study are available from the corresponding author upon reasonable request.

Results

Histological alterations are sensitive markers that can be used to detect the noxious effects of various substances on different organs including the skin. Here, we sought to design a pipeline (called NoxiScore) for automated detection of nuclear morphology in skin histological sections and accurate quantification of nuclear abnormalities following exposure to stress or dermato-cosmetic products.

Design of the NoxiScore workflow

The technique used to assess the histological integrity or damage involves including ex vivo cultured skin samples in paraffin followed by coloration with hematoxylin and eosin. The bio-image analysis pipeline (Fig. 1) starts with the capture of images collected using high-resolution light microscopy of human skin samples submitted

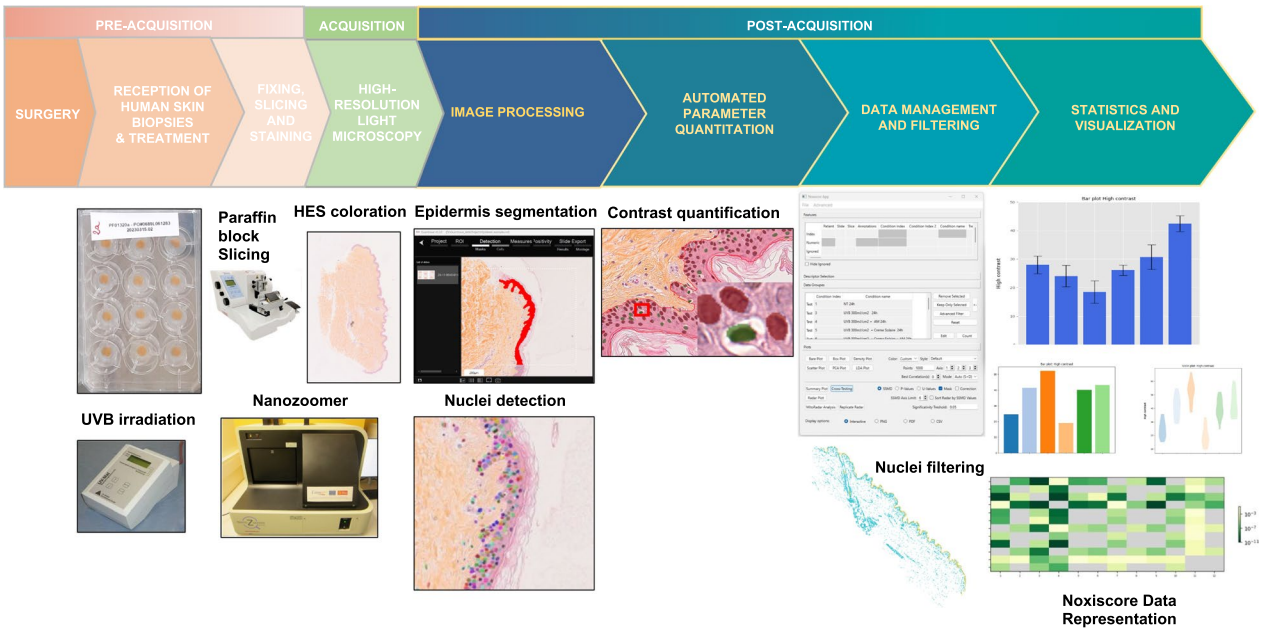

Fig. 1 NoxiScore image analysis pipeline for nuclei analysis in histological images of ex vivo skin samples. The figure describes a new methodology for quantitative characterization of nuclear appearance in large-scale whole-slide microscopic images using human skin explants as seed material. Schematic view of the system involving pre-acquisition (treatment and preparation of the biological material), acquisition (on a modern slide scanner producing high-resolution images within minutes), and post-acquisition steps (including segmentation and feature computation). Large-scale computerized slides are taken from hematoxylin and eosin (HE) [or hematoxylin-eosin saffron (HES)] stained permanent sections of formalin-fixed and paraffin-embedded tissues. Our in-house software (NoxiScore) then handles all fundamental operations from image segmentation to statistical analysis. NoxiScore software uses deep learning during the image segmentation phase and calculates about a dozen morphological descriptors (Additional file 3). A graphical interface facilitates data collection, handling and processing

to different treatments. The NoxiScore software relies on two segmentation methods with deep learning for, respectively, epidermis and nuclei segmentation. The segmentation procedure focuses on extracting foreground objects of interest, i.e. nuclei or epidermis, from background areas. In the post-processing step, unsatisfying detected objects can be filtered out (e.g. non-epidermal nuclei are automatically removed). Segmentation is followed by computation of different categories of nuclear features, such as size, shape, intensity, texture and gradient statistics (which the human eye has difficulty perceiving). An automatic algorithm was written to compute these morphometric parameters from the produced binary segmented images. Description of the quantitative parameters generated by NoxiScore can be found in Additional file 3. Statistical analysis, as well as tables, are integrated into a user-friendly interface.

Digital morphometric analysis of skin biopsies treated with hydrogen peroxide identifies a discriminating feature of histological alterations

First, we set out to identify the nuclear morphometric features significantly correlated with histological alterations in our ex vivo skin model. Skin explants were exposed to slight hydrogen peroxide (H_2O_2) treatment as a procedure to cause superficial oxidative stress [67–71]. The morphology of the control skin was in accordance with what is normally observed in healthy conditions, with all epidermal layers, the stratum basale, stratum spinosum, stratum granulosum and stratum corneum, appearing intact [72, 73]. Skin sections from the in vivo trial sampled at 24 h post-H_2O_2 exposure were compared to the control. Despite their similar overall visual appearance at the tissue level, the treated samples exhibited more condensed and darker nuclei (indicative of pyknosis) compared to the control samples (Fig. 2A). Next, we derived histograms of mean values associated with ten individual features and investigated which of these were most discriminant between the experimental conditions (Additional file 3). Noticeably, our data revealed that one of the texture parameters, namely the Gray Level Co-occurrence Matrix of contrast (GLCM contrast, herein referred to as "High Contrast Mean" or HCM), was best at discriminating between intact and H_2O_2-exposed skin samples (Fig. 2B). This parameter, known to be an efficient descriptor for discriminating different textural patterns [74], measures the average gray level difference between neighbor pixels (i.e. the amount of local variation between a contiguous set of pixels). In the context of our histo-morphological approach, this feature (expressed as a percentage) shows a statistically significant overabundance of nuclei surrounded by a clear halo or empty space (black arrows in Fig. 2A, panel b) in treated skin explants. Skin cells appeared partially vacuolated and disordered. Careful examination of H_2O_2-exposed skin sections further revealed that these nuclei enclosed within a circular or elliptical hollow

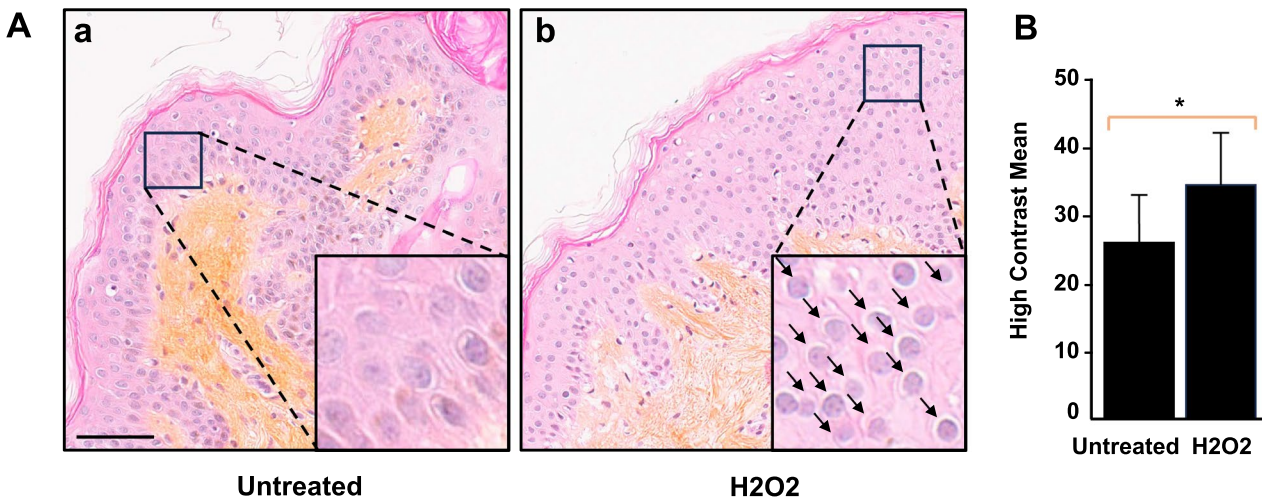

Fig. 2 Histometric analysis of human skin biopsies treated with hydrogen peroxide. **A** Histological characterization of skin explants (8 mm diameter) exposed to hydrogen peroxide (H_2O_2) 24 h during ex vivo culture; 3-µm skin cross-sections of fresh human skin fixed with 10% buffered formalin and embedded in paraffin wax. Hematoxylin-eosin saffron (HES) staining. Magnification is 20× (scale bar: 50 µM). All different layers of the epidermis were detected with the purple staining of nuclei in the pink cellular background. A bright line is visible at the top of the skin that corresponds to the stratum corneum. Dermis (collagen fibers) appears in orange. Inset details show the areas of interest with haloed nuclei indicated by arrows. **B** Histograms showing high contrast mean values (expressed in percent) between untreated and H_2O_2-treated human skin explants with a total of 80,914 analyzed nuclei. The number of nuclei analyzed per condition is given in Additional file 4. Results are from triplicate biopsies from the same donor. Standard Student's t-test was used to measure significance between two groups

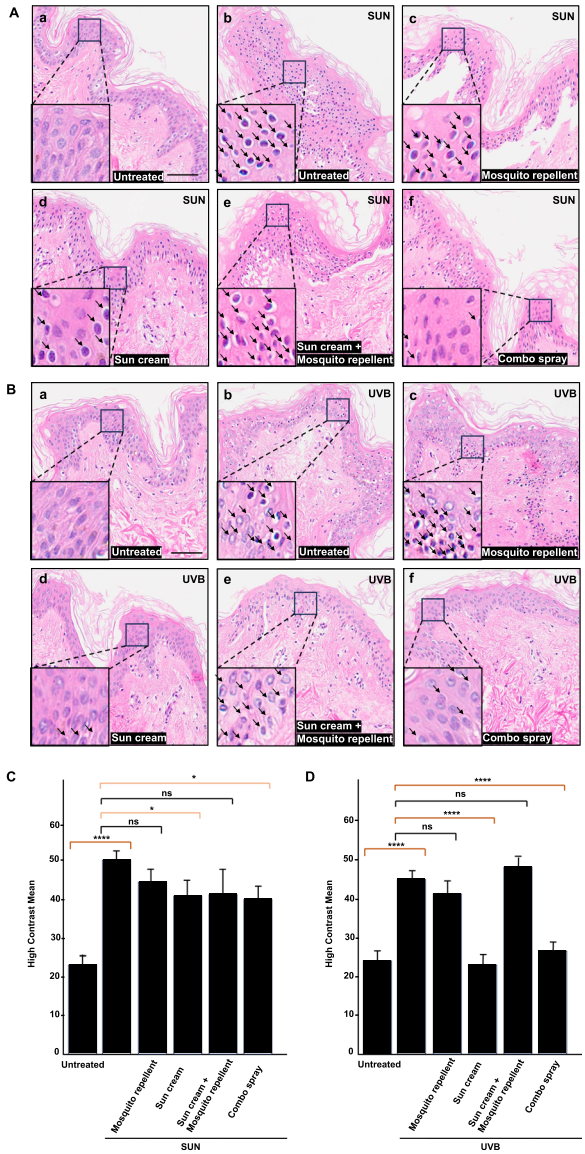

◀ **Fig. 3** Histometric analysis of skin biopsies from a single donor treated with repellent and sunscreen formulations. Skin samples (from the same donor) were treated with (i) a sunscreen containing UV filters (panels Ad and Bd) and/or (ii) a mosquito repellent with synthetic active ingredient IR3535 (panels Ac and Bc) or (iii) a commercial preparation of a natural insect repellent plus sunscreen ('combo') (panels Af and Bf). The treated skin biopsies were exposed to outdoor sunlight (**A**) or to UVB irradiation in controlled conditions (**B**). Hematoxylin-eosin (HE) staining. Scale bar: 50 µM. Inset details show the areas of interest with haloed nuclei indicated by arrows. Separate treatment with the insect repellent (**c**) or the sunscreen (**d**) used as single products before sunlight exposure (2 h, UV index 8) (**A**) or UVB irradiation (**B**). Concurrent application of the insect repellent with the sunscreen. Treatment with a combination of sunscreen and insect repellent (in layers, first sunscreen and then insect repellent) (**e**). Treatment with a commercial preparation of a natural insect repellent plus sunscreen ('combo') (**f**). Histograms showing high contrast mean values between untreated and treated human skin explants exposed to solar radiation (**C**) or laboratory UVB irradiation (**D**). Results are from triplicate biopsies from a unique donor. Standard Student's t-test was used to compare samples. A total of 1,185,854 nuclei were analyzed, and details of nucleus counting per condition is given in Additional file 4

area were mainly found in the stratum spinosum (the epidermal layer where desmosomes form between adjacent keratinocytes). We interpret HCM deviation from the reference situation as indicative of tissue injury due to toxic damage to cells, with the appearance of pyknotic nuclei (darker, condensed) indicating the onset of cell death processes.

Nuclear contour based approach suggests that applying a commercial insect repellent lowers the efficacy of a popular sunscreen

Having identified a potentially relevant histological correlate of stress in ex vivo skin samples, we examined whether our pipeline could be useful in evaluating efficacy and safety of insect repellents and sunscreens administered individually or in combination. Skin samples (from the same donor) were treated with (i) a sunscreen containing UV filters and/or (ii) a mosquito repellent with synthetic active ingredient IR3535 (sunscreen first, followed by a mosquito repellent in case of combined application) or (iii) a commercial preparation of a natural insect repellent plus sunscreen ('combo'); these three products were sold extensively at the time of the study (spring and summer 2022) in the Montpellier area (South of France). The treated skin biopsies were exposed to UVB irradiation (in the laboratory) or to sunlight (in real-life settings). Histological investigation by HE staining showed that haloed nuclei were particularly visible 24 h after sun or UVB exposure with an even distribution (Fig. 3A and B, b panels). This result suggests that UV irradiation induced alterations in the skin explants, which was confirmed using quantitative assessment of HCM values in control versus exposed samples (Fig. 3C and D; Additional file 3). As expected, this nuclear contour score was significantly reduced (Fig. 3C) and even brought to the same levels detected in unexposed skin samples (Fig. 3D) when the sunscreen was applied as a separate treatment before sunlight exposure or UVB irradiation, respectively (Fig. 3C and D). In contrast, application of the mosquito repellent as a single product did not exert any protective effect against UVB or sun exposure. Histology nicely corroborated the quantifications (panels e in Fig. 3A and B, C and D), showing that the sunscreen efficiently blocked UV radiation.

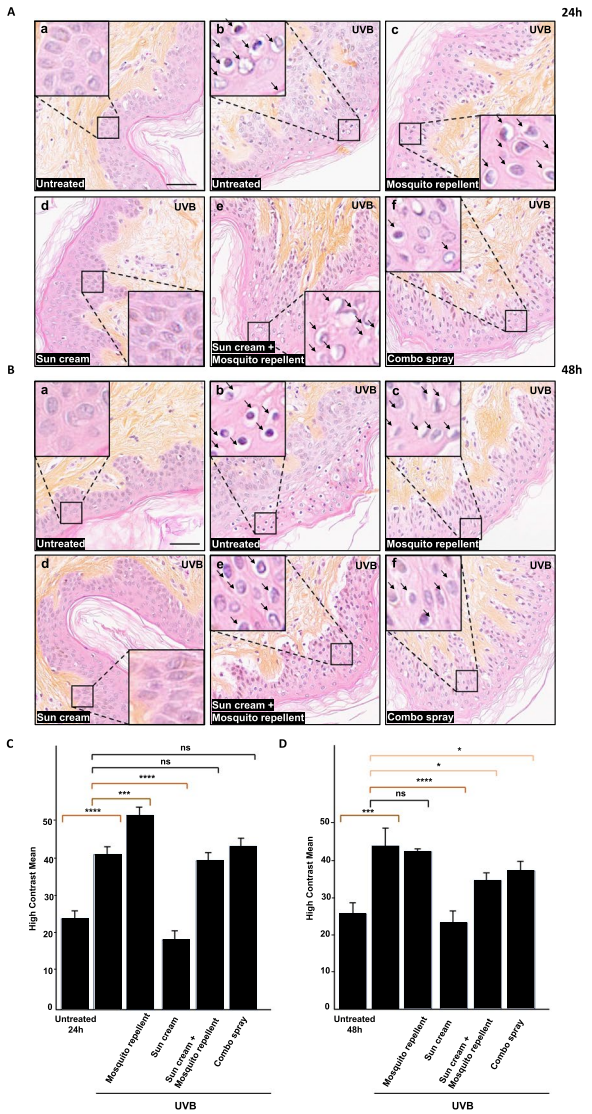

◀ **Fig. 4** Histometric analysis of skin biopsies from multiple donors treated with repellent and sunscreen formulations. Skin samples (from the same donor) were treated with (i) a sunscreen containing UV filters and/or (ii) a mosquito repellent with synthetic active ingredient IR3535 or (iii) a commercial preparation of a natural insect repellent plus sunscreen ('combo'). The treated skin biopsies were exposed to outdoor sunlight (**A**) or to UVB irradiation in controlled conditions (**B**). Hematoxylin-eosin saffron (HES) staining. Scale bar: 50 µM. Inset details show the areas of interest with haloed nuclei indicated by arrows. Separate treatment with the insect repellent (**c**) or the sunscreen (**d**) used as single products before sunlight exposure (UV index 8) or UVB irradiation (300 mJ/cm^2). Concurrent application (**e**) of the insect repellent with the sunscreen. Treatment with a combination of sunscreen and insect repellent (in layers, first sunscreen and then insect repellent) (**e**). Treatment with a commercial preparation of a natural insect repellent plus sunscreen ('combo') (**f**). Histograms showing high contrast mean values between untreated and treated human skin explants exposed to laboratory UVB irradiation for 24 h (**C**) or 48 h (**D**). Results are from triplicate biopsies from three different donors. Standard Student's t-test was used to compare samples. A total of 725,397 nuclei were analyzed, and details of nuclei counting per condition are given in Additional file 4

Interestingly, concurrent application of the insect repellent spray with the commercial sun cream significantly reduced the UVB protective effect of the sunscreen (Fig. 3C) and even obliterated protection in case of sun exposure (Fig. 3C). Last, the sunscreen-insect repellent combo product showed moderate protection against solar radiation (Fig. 3A panel f and Fig. 3C), whereas it completely blocked the effects of UVB irradiation based on the relative absence of haloed nuclei in combination-treated skin samples (Fig. 3B panel f) and computed HCM values that were similar to unexposed samples from the assayed donor (Fig. 3D). Note that sunscreen formulations may exhibit narrow spectrum protection, covering mostly UVB and providing less photoprotection against UVA and possibly other rays of the solar spectrum.

Distinct histological and histometric effects of individual synthetic insect repellent and sunscreen products compared to combo spray

In a third set of experiments, the number of donors was raised to $N=3$, and histological analysis was conducted by HES (to better separate the epidermis from the dermis) at both 24 h and 48 h after UVB irradiation. Agreeing with the results described in the previous section, UVB exposure had a significant impact on the detection of haloed nuclei (Fig. 4A and B, b panels), the proportion of which doubled post-UVB irradiation based on HCM quantification (Fig. 4C and D). Cells in the deep epidermal layers appeared partially vacuolated and irregularly arranged. Application of the sunscreen as a single product provided complete protection against UVB effects (Fig. 4A and B, d panels and Fig. 4C and D), whereas separate application of the insect repellent enhanced the effects of UVB exposure (evaluated 24 h post-irradiation) or tended to be neutral against UVB treatment (at 48 h) (Fig. 4A and B, c panels and Fig. 4C and D). Here again, concomitant application of the insect repellent with the sunscreen impaired or significantly diminished its protective effect against UVB (Fig. 4A and B, e panels and Fig. 4C and D). Contrary to the previous experiment, the results indicate that the sunscreen-insect repellent combo had a null (Fig. 4A panel f, at 24 h post-UVB irradiation) or limited impact (Fig. 4B panel f, 48 h) on the number of haloed nuclei and related HCM parameter

values (Fig. 4C and D). This inter-individual heterogeneity in the responses may be linked to donor-to-donor variability in skin explants.

Discussion

In recent years, interest has grown in computer-assisted morphometry to investigate the cellular and nuclear changes correlated with the physio-pathological status of histologically stained sections [39–53]. Artificial intelligence has also moved to the forefront of digital histology, bringing opportunities in terms of reliability, objectivity and reproducibility [75, 76]. At the nuclear level, morphological phenotypes were usually qualitatively described through visual clues as 'abnormal' or 'dysmorphic,' which was low throughput and often subjected to observer bias. Quantitative, feature-based approaches now allow for quick analysis of large sets of imaging data through an automated process and can extend the scope of descriptive features beyond those readily perceived by the human eye [77]. In the present study, we developed NoxiScore, a pipeline providing an integrated, deep learning-based software solution for fully automated and quantitative analysis of nuclear shape in HE-stained images of human skin biopsies. A number of easy-to-compute features can reveal the presence of nuclear singularities. These include a novel indicator herein named HCM (for high contrast mean) that relates to the haloed shape of nuclei in UV-exposed epidermal regions of human skin cross-sections. Such nuclei surrounded by a clear empty space could be seen in various publications dealing with skin histology (see for instance Fig. 2 in Han et al. [23]). While already known as a texture feature [78–80], most programs and studies were interested in analyzing the nucleus per se and not its surrounding space, which probably explains why deviations in this specific parameter went largely unnoticed in previous studies. Our wet-plus-dry technology based on computational histology of human skin explants may be useful for drug screening purposes, safety testing, evaluating health risks associated with exposure to environmental chemicals, the pharmaco-toxicological assessment of active ingredients and formulations and cell cultures and reconstructed skin models. To examine the effects of various test substances on the epidermis, viability assays [e.g. MTT or lactate dehydrogenase (LDH) assays] and immunohistochemical (IHC) staining are classically performed. However, these techniques are very expensive and time-consuming, especially when conducted for many specific biomarkers. Future research is needed to determine whether quantification of HCM values could represent a relevant and convenient biomarker that changes primarily with cellular injury in the ex vivo human skin model. To this end, correlation between HCM values and the percentage of pyknotic nuclei (often characterized by their condensed, shrunken, irregular, non-spherical shape and darker shade) or other cell death indicators (e.g. caspase-3 activation in the case of apoptosis evaluation) will have to be formally investigated in future studies. Evaluation of a greater number of donors will be essential to determine the robustness of this parameter (i.e. sensitivity and specificity) prior to its establishment as a formal indicator of epidermal damage. Notably, although we presented our histometric framework with application to skin explants, it could potentially be tailored to a broad scope of tissues since many classification schemes rely on nuclear feature analysis.

Insect repellent is one of the major preventive methods against mosquito-borne diseases, while sunscreens help prevent sunburns and skin cancers. These products are particularly crucial for travelers and other people who engage in outdoor activities and are exposed to both mosquito stings and solar radiation. People who engage in outdoor activities and those who live in sunny areas with many insects including mosquitoes (such as in the Languedoc coastal region and near Camargue, southern France) are often tempted to overuse these products, especially on hotter or windier days. Formulations containing different active ingredients in various concentrations are available on the market. Sunscreens and insect repellents are often used together and combined for ease of use in some commercial 'combo' products. However, toxicity information on combination use is currently limited, although there are research studies on efficacy testing. The observations presented here suggest that, based on histological analysis and HCM scores, dual application of a popular synthetic insect repellent (containing IR3535) with a widely distributed commercial sunscreen induced a significant decrease in the protective effects against UV exposure. A similar finding was reported for DEET (N,N-diethyl-meta-toluamide), which was found to hinder the efficacy of sunscreen when used concurrently [21, 81] (in addition to being a skin irritant [23]). Here, addition of an insect repellent containing botanical extracts to the sunscreen formulation led to heterogeneous results in terms of photoprotection, probably due to inter-donor variations. Plant-based insect repellents have been reported to be less effective with shorter durations of protection compared to their synthetic equivalents, and some may be noxious if used for longer duration [82, 83]. At the same time, co-administration of a synthetic insect repellent like DEET together with other chemical substances, such as the sunscreen compound oxybenzone [19, 20, 84, 85], is suspected to increase absorption of all topically applied products (including pesticides [86]) and to pose a health risk. For topical preparations containing combinations of natural or synthetic repellents with

sunscreen, the frequency of application may also be an issue because insect repellents should be reapplied less often than sunscreens [87]. Note that absolute evaluation of these results is difficult since the final products contain small amounts of ingredients along with many other ingredients (Additional file 2). It will also be necessary to implement other application protocols, such as applying mixtures of products instead of layering, to confirm our conclusions. Last, certain products may prove to be toxic in the ex vivo model but non-toxic in vivo, or ex vivo findings may overestimate the direct effects expected in vivo. Although skin explants give a better representation of the in vivo milieu and cell composition than in vitro cultured cells, understanding the specific limitations of our ex vivo pipeline, combining it with in vivo studies when feasible and considering the potential impact of the application protocols, may help devise more advanced future studies.

Conclusions

To our knowledge, our study is the first to evaluate the potential toxicity of combining real-life sunscreen and insect repellent formulations in an ex vivo human skin model, which provides the closest representation of the cutaneous physiology. The described methodology has the potential to inform health policy guidelines and end users on how to chose effective and safe insect repellents and sunscreens from the vast spectrum of commercially available products.

Supplementary Information

The online version contains supplementary material available at https://doi.org/10.1186/s13071-025-06712-3.

Additional file 1. Information on biological material. Synthesis of the information displayed on the Genoskin batch release certificates.

Additional file 2. Ingredient lists of the products used in the study.

Additional file 3. Histograms showing mean values of the different morphometric parameters computed by NoxiScore. Skin samples (from the same donor) were treated or not (first two lines of each histogram; two biopsies from the same patient) with a sunscreen containing UV filters (line 4 of each histogram) or a mosquito repellent with synthetic active ingredient IR3535 (line 5 of each histogram) 30 min before exposure to UVB irradiation in controlled conditions (lines 3, 4 and 5 of each histogram). Histograms showing quantification of nuclei parameters including area, perimeter, roundness, intensities maximum, minimum and mean, GLCM contrast, energy, entropy and homogeneity 24 h after UVB irradiation. Results are from triplicate biopsies from a unique donor. Standard t-test was used to compare samples.

Additional file 4. Nuclei counting and parameter quantification per condition. The number of nuclei shows the number of cells analyzed.

Acknowledgements

We thank Sébastien Picard, Sébastien Gibert and Florence Saïdani at ISEM for their support. We also thank Jérôme Perez and Marine Ledru at ISEM and Gaetan Galisot and Damien Blanc at QuantaCell for their help. The authors are grateful to Patricia Verwaerde (DR13 CNRS). We acknowledge the imaging facility MRI, a member of the France-BioImaging national infrastructure supported by the French National Research Agency (ANR-10-INBS-04, "Investments for the future"). We acknowledge the "Réseau d'Histologie Expérimentale de Montpellier" (RHEM facility), supported by SIRIC Montpellier Cancer (Grant INCa_Inserm_DGOS_12553), the European regional development foundation and the Occitanie region (FEDER-FSE 2014-2020 Languedoc Roussillon), for processing our tissues and their histology techniques and expertise. Special thanks go to Nelly Pirot and Alicia Seguin for their expert assistance.

Author contributions

SC: Data curation; formal analysis; investigation; visualization; methodology; writing—review and editing. TP: Data curation; software; formal analysis; investigation; visualization; methodology. CSO: Data curation; formal analysis; investigation; visualization; methodology. MW: Resources; data curation; methodology; writing—review and editing. AS: Resources; data curation; methodology; writing—review and editing. VR: Data curation; software; formal analysis; investigation; visualization; methodology. AA: Conceptualization; data curation; formal analysis; supervision; funding acquisition; investigation; visualization; writing—original draft; project administration; writing—review and editing. All authors read and approved the final manuscript.

Funding

This work was funded by the French "Plan de relance" (CNRS no. 234144) jointly with QuantaCell and by the project ANR-24-CE34-1332.

Availability of data and materials

The data that support the findings of this study are available on request from the corresponding author. Software for this research is not publicly available due to possible future commercial exploitation.

Declarations

Ethics approval and consent to participate

Not applicable.

Consent for publication

Not applicable.

Competing interests

The authors declare no competing interests.

Author details

[1]ISEM, Univ Montpellier, CNRS, IRD, Montpellier, France. [2]QuantaCell SAS, Hôpital Saint Eloi, IRMB, 80 Av Augustin Fliche, 34090 Montpellier, France. [3]EDENCOS, 39 Ancienne Route Nationale 7, 69570 Dardilly, France.

Received: 19 November 2024 Accepted: 4 February 2025
Published online: 04 March 2025

References

1. Brettmann EA, de Guzman SC. Recent evolution of the human skin barrier. Exp Dermatol. 2018;27:859–66.
2. Elias PM, Menon G, Wetzel BK, Williams JJW. Barrier requirements as the evolutionary 'driver' of epidermal pigmentation in humans. Am J Hum Biol. 2010;22:526–37.
3. Baker P, Huang C, Radi R, Moll SB, Jules E, Arbiser JL. Skin barrier function: the interplay of physical, chemical, and immunologic properties. Cells. 2023;12:2745.
4. Madison KC. Barrier function of the skin: 'la raison d'être' of the epidermis. J Invest Dermatol. 2003;121:231–41.
5. Matsui T, Amagai M. Dissecting the formation, structure and barrier function of the stratum corneum. Int Immunol. 2015;27:269–80.
6. Lingeman DG, O'Dell KL, Syed Z. Developing attractants and repellents for ticks: promises and challenges. Curr Opin Insect Sci. 2024;63:101181.
7. Duval P, Aschan-Leygonie C, Valiente MC. A review of knowledge, attitudes and practices regarding mosquitoes and mosquito-borne

infectious diseases in nonendemic regions. Front Pub Health. 2023;11:1239874.
8. WHO TEAM Control of Neglected Tropical Diseases (NTD. Guidelines for efficacy testing of mosquito repellents for human skin. World Health Organization; 2009 p. 1–37. Report No.: WHO/HTM/NTD/WHOPES/2009.4. https://iris.who.int/bitstream/handle/10665/70072/WHO_HTM_NTD_WHOPES_2009.4_eng.pdf?sequence=1. Accessed 2 Apr 2024.
9. Nguyen QBD, Vu MAN, Hebert AA. Insect repellents: an updated review for the clinician. J Am Acad Dermatol. 2023;88:123–30.
10. Lupi E, Hatz C, Schlagenhauf P. The efficacy of repellents against *Aedes*, *Anopheles*, *Culex* and *Ixodes* spp.—a literature review. Travel Med Infect Dis. 2013;11:374–411.
11. Katz TM, Miller JH, Hebert AA. Insect repellents: historical perspectives and new developments. J Am Acad Dermatol. 2008;58:865–71.
12. Fathy Khater H, Selim AM, Abouelella GA, Abouelella NA, Murugan K, Vaz NP, et al. Commercial mosquito repellents and their safety concerns. In: Kasenga FH, editor., et al., Malaria. London: IntechOpen; 2019.
13. Lee MY. Essential oils as repellents against arthropods. Biomed Res Int. 2018;2018:6860271.
14. Juckett G. Arthropod-borne diseases: the camper's uninvited guests. Microbiol Spectr. 2015;3(4). https://doi.org/10.1128/microbiolspec.IOL5-0001-2014. PMID: 26350321.
15. Snyder A, Valdebran M, Terrero D, Amber KT, Kelly KM. Solar ultraviolet exposure in individuals who perform outdoor sport activities. Sports Med Open. 2020;6:42.
16. Raymond-Lezman JR, Riskin S. Attitudes, behaviors, and risks of sun protection to prevent skin cancer amongst children, adolescents, and adults. Cureus. 2023;15:e34934.
17. Powers JM, Murphy JEJ. Sunlight radiation as a villain and hero: 60 years of illuminating research. Int J Radiat Biol. 2019;95:1043–9.
18. McDonald KA, Lytvyn Y, Mufti A, Chan AW, Rosen CF. Review on photoprotection: a clinician's guide to the ingredients, characteristics, adverse effects, and disease-specific benefits of chemical and physical sunscreen compounds. Arch Dermatol Res. 2023;315:735–49.
19. Gu X, Wang T, Collins DM, Kasichayanula S, Burczynski FJ. In vitro evaluation of concurrent use of commercially available insect repellent and sunscreen preparations. Br J Dermatol. 2005;152:1263–7.
20. Wang T, Gu X. In vitro percutaneous permeation of the repellent DEET and the sunscreen oxybenzone across human skin. J Pharm Pharm Sci. 2007;10:17–25.
21. Rodriguez J, Maibach HI. Percutaneous penetration and pharmacodynamics: wash-in and wash-off of sunscreen and insect repellent. J Dermatolog Treat. 2016;27:11–8.
22. Kasichayanula S, House JD, Wang T, Gu X. Percutaneous characterization of the insect repellent DEET and the sunscreen oxybenzone from topical skin application. Toxicol Appl Pharmacol. 2007;223:187–94.
23. Han JS, Kim YB, Park H, Im WJ, Kim WJ, Kim Y, et al. In vitro skin irritation assessment using EpiDerm™: applicability for updating toxicity information of oxybenzone and N N-diethyl-m-toluamide. Drug Chem Toxicol. 2020;43:361–8.
24. Strickland J, Haugabrooks E, Allen DG, Balottin LB, Hirabayashi Y, Kleinstreuer NC, et al. International regulatory uses of acute systemic toxicity data and integration of new approach methodologies. Crit Rev Toxicol. 2023;53:385–411.
25. Pistollato F, Madia F, Corvi R, Munn S, Grignard E, Paini A, et al. Current EU regulatory requirements for the assessment of chemicals and cosmetic products: challenges and opportunities for introducing new approach methodologies. Arch Toxicol. 2021;95:1867–97.
26. Arnesdotter E, Rogiers V, Vanhaecke T, Vinken M. An overview of current practices for regulatory risk assessment with lessons learnt from cosmetics in the European Union. Crit Rev Toxicol. 2021;51:395–417.
27. Kim KB, Kwack SJ, Lee JY, Kacew S, Lee BM. Current opinion on risk assessment of cosmetics. J Toxicol Environ Health B Crit Rev. 2021;24:137–61.
28. Kandárová H, Hayden P, Klausner M, Kubilus J, Sheasgreen J. An in vitro skin irritation test (SIT) using the EpiDerm reconstructed human epidermal (RHE) model. J Vis Exp. 2009;29:1366.
29. Kojima H, Ando Y, Idehara K, Katoh M, Kosaka T, Miyaoka E, et al. Validation study of the in vitro skin irritation test with the LabCyte EPI-MODEL24. Altern Lab Anim. 2012;40:33–50.
30. Alépée N, Tornier C, Robert C, Amsellem C, Roux MH, Doucet O, et al. A catch-up validation study on reconstructed human epidermis (SkinEthic RHE) for full replacement of the Draize skin irritation test. Toxicol In Vitro. 2010;24:257–66.
31. Tammi R, Maibach H. Skin organ culture: why? Int J Dermatol. 1987;26:150–60.
32. Moll I. Human skin organ culture. Methods Mol Med. 2003;78:305–10.
33. Zhao H, Chen Z, Kang X, Yang B, Luo P, Li H, et al. The frontline of alternatives to animal testing: novel in vitro skin model application in drug development and evaluation. Toxicol Sci. 2023;196:152–69.
34. Filaire E, Nachat-Kappes R, Laporte C, Harmand MF, Simon M, Poinsot C. Alternative in vitro models used in the main safety tests of cosmetic products and new challenges. Int J Cosmet Sci. 2022;44:604–13.
35. Zhou L, Ji W, Dicolandrea T, Finlay D, Supp D, Boyce S, et al. An improved human skin explant culture method for testing and assessing personal care products. J Cosmet Dermatol. 2023;22:1585–94.
36. Charrasse S, Racine V, Saint-Omer C, Poquillon T, Lionnard L, Ledru M, et al. Quantitative imaging and semiotic phenotyping of mitochondrial network morphology in live human cells. PLoS ONE. 2024;19:e0301372.
37. Charrasse S, Poquillon T, Saint-Omer C, Pastore M, Bordignon B, Frye RE, et al. Quantitative assessment of mitochondrial morphology relevant for studies on cellular health and environmental toxicity. Comput Struct Biotechnol J. 2023;21:5609–19.
38. Jugé R, Breugnot J, Da Silva C, Bordes S, Closs B, Aouacheria A. Quantification and characterization of UVB-induced mitochondrial fragmentation in normal primary human keratinocytes. Sci Rep. 2016;6:35065.
39. Carleton NM, Lee G, Madabhushi A, Veltri RW. Advances in the computational and molecular understanding of the prostate cancer cell nucleus. J Cell Biochem. 2018;119:7127–42.
40. Bacus JW. Cervical cell recognition and morphometric grading by image analysis. J Cell Biochem Suppl. 1995;23:33–42.
41. Dawson AE, Austin RE, Weinberg DS. Nuclear grading of breast carcinoma by image analysis. Classification by multivariate and neural network analysis. Am J Clin Pathol. 1991;95:S29-37.
42. Chan HP, Doi K, Galhotra S, Vyborny CJ, MacMahon H, Jokich PM. Image feature analysis and computer-aided diagnosis in digital radiography. I. Automated detection of microcalcifications in mammography. Med Phys. 1987;14:538–48.
43. Green A, Martin N, Pfitzner J, O'Rourke M, Knight N. Computer image analysis in the diagnosis of melanoma. J Am Acad Dermatol. 1994;31:958–64.
44. Zink D, Fischer AH, Nickerson JA. Nuclear structure in cancer cells. Nat Rev Cancer. 2004;4:677–87.
45. Wang W, Ozolek JA, Rohde GK. Detection and classification of thyroid follicular lesions based on nuclear structure from histopathology images. Cytometry A. 2010;77:485–94.
46. Raju Ragavendra T, Rammanohar M, Sowmya K. Morphometric computer-assisted image analysis of oral epithelial cells in normal epithelium and leukoplakia. J Oral Pathol Med. 2010;39:149–54.
47. Fidziańska A, Hausmanowa-Petrusewicz I. Architectural abnormalities in muscle nuclei. Ultrastructural differences between X-linked and autosomal dominant forms of EDMD. J Neurol Sci. 2003;210:47–51.
48. Sabatelli P, Lattanzi G, Ognibene A, Columbaro M, Capanni C, Merlini L, et al. Nuclear alterations in autosomal-dominant Emery-Dreifuss muscular dystrophy. Muscle Nerve. 2001;24:826–9.
49. Lammerding J, Hsiao J, Schulze PC, Kozlov S, Stewart CL, Lee RT. Abnormal nuclear shape and impaired mechanotransduction in emerin-deficient cells. J Cell Biol. 2005;170:781–91.
50. Dahl KN, Scaffidi P, Islam MF, Yodh AG, Wilson KL, Misteli T. Distinct structural and mechanical properties of the nuclear lamina in Hutchinson-Gilford progeria syndrome. Proc Natl Acad Sci U S A. 2006;103:10271–6.
51. Eriksson M, Brown WT, Gordon LB, Glynn MW, Singer J, Scott L, et al. Recurrent de novo point mutations in lamin A cause Hutchinson-Gilford progeria syndrome. Nature. 2003;423:293–8.
52. Kemeny S, Tatout C, Salaun G, Pebrel-Richard C, Goumy C, Ollier N, et al. Spatial organization of chromosome territories in the interphase nucleus of trisomy 21 cells. Chromosoma. 2018;127:247–59.
53. Paonessa F, Evans LD, Solanki R, Larrieu D, Wray S, Hardy J, et al. Microtubules deform the nuclear membrane and disrupt nucleocytoplasmic transport in tau-mediated frontotemporal dementia. Cell Rep. 2019;26:582-593.e5.
54. Abadie S, Jardet C, Colombelli J, Chaput B, David A, Grolleau JL, et al. 3D imaging of cleared human skin biopsies using light-sheet microscopy:

a new way to visualize in-depth skin structure. Skin Res Technol. 2018;24:294–303.
55. De Wever B, Kurdykowski S, Descargues P. Human skin models for research applications in pharmacology and toxicology: introducing NativeSkin ®, the "missing link" bridging cell culture and/or reconstructed skin models and human clinical testing. Appl In Vitro Toxicol. 2015;1:26–32.
56. U.S Centers for disease control and prevention. Preventing Mosquito Bites [Internet]. Available from: https://www.cdc.gov/mosquitoes/prevention/index.html
57. U.S Centers for disease control and prevention. Sun Exposure. https://wwwnc.cdc.gov/travel/page/sun-exposure
58. Genoskin ex vivo clinical testing. NativeSkin® NativeSkin® Access User manual. https://www.genoskin.com/wp-content/uploads/2020/09/Genoskin_manuel_NativeSkin-Access-V4.pdf. Accessed 31 May 2022.
59. Dezest M, Le Bechec M, Chavatte L, Desauziers V, Chaput B, Grolleau JL, et al. Oxidative damage and impairment of protein quality control systems in keratinocytes exposed to a volatile organic compounds cocktail. Sci Rep. 2017;7:10707.
60. Vind AC, Wu Z, Firdaus MJ, Snieckute G, Toh GA, Jessen M, et al. The ribotoxic stress response drives acute inflammation, cell death, and epidermal thickening in UV-irradiated skin in vivo. Mol Cell. 2024;84:4774-4789.e9.
61. Reefman E, Kuiper H, Jonkman MF, Limburg PC, Kallenberg CGM, Bijl M. Skin sensitivity to UVB irradiation in systemic lupus erythematosus is not related to the level of apoptosis induction in keratinocytes. Rheumatology. 2006;45:538–44.
62. Straface E, Vona R, Ascione B, Matarrese P, Strudthoff T, Franconi F, et al. Single exposure of human fibroblasts (WI-38) to a sub-cytotoxic dose of UVB induces premature senescence. FEBS Lett. 2007;581:4342–8.
63. Khouri-Saba P, Vandecreme A, Brady M, Bhadriraju K, Bajcsy P. Deep Zoom tool for advanced interactivity with high-resolution images. SPIE Newsroom. 2013. http://www.spie.org/x93885.xml. Accessed 9 Jan 2025.
64. Ronneberger O, Fischer P, Brox T. U-Net: convolutional networks for biomedical image segmentation. In: Navab N, Hornegger J, Wells WM, Frangi AF, editors. Medical image computing and computer-assisted intervention—MICCAI 2015, vol. 9351. Lecture Notes in Computer Science. Cham: Springer International Publishing; 2015. p. 234–41. https://doi.org/10.1007/978-3-319-24574-4_28.
65. Schmidt U, Weigert M, Broaddus C, Myers G. Cell detection with star-convex polygons. In: Frangi AF, Schnabel JA, Davatzikos C, Alberola-López C, Fichtinger G, editors. Medical image computing and computer assisted intervention—MICCAI 2018, vol. 11071. Lecture Notes in Computer Science. Cham: Springer International Publishing; 2018. p. 265–73. https://doi.org/10.1007/978-3-030-00934-2_30.
66. Haralick RM, Shanmugam K, Dinstein I. Textural features for image classification. IEEE Trans Syst, Man, Cybern. 1973;3:610–21.
67. El Hindi T, Ehlers G, Demchuk M, Pfitzner I. Determination of the antioxidant capacity of an antioxidant combination using the fluoroscan assay in vitro and visualization of its effects using histological methods. Arch Dermatol Res. 2004;296:258–64.
68. Reid L, Clothier RH, Khammo N. Hydrogen peroxide induced stress in human keratinocytes and its effect on bithionol toxicity. Toxicol In Vitro. 2001;15:441–5.
69. Murphy EC, Friedman AJ. Hydrogen peroxide and cutaneous biology: Translational applications, benefits, and risks. J Am Acad Dermatol. 2019;81:1379–86.
70. Ben Khedir S, Moalla D, Jardak N, Mzid M, Sahnoun Z, Rebai T. *Pistacia lentiscus* fruit oil reduces oxidative stress in human skin explants caused by hydrogen peroxide. Biotech Histochem. 2016;91:480–91.
71. Dammak I, Abdallah FB, Boudaya S, Besbes S, Keskes L, Gaied AE, et al. Date seed oil limit oxidative injuries induced by hydrogen peroxide in human skin organ culture. BioFactors. 2007;29:137–45.
72. Ng KW, Lau WM. Skin deep: the basics of human skin structure and drug penetration. In: Dragicevic N, Maibach HI, editors. Percutaneous penetration enhancers chemical methods in penetration enhancement. Berlin, Heidelberg: Springer, Berlin Heidelberg; 2015. p. 3–11. https://doi.org/10.1007/978-3-662-45013-0_1.
73. Griffiths C, Barker J, Bleiker T, Hussain W, Simpson RC. Rook's textbook of dermatology. 10th ed. Hoboken: Wiley-Blackwell; 2024. p. 1.
74. Wang Z, Bovik AC, Lu L. Why is image quality assessment so difficult? In: IEEE International Conference on Acoustics Speech and Signal Processing. Orlando, FL, USA: IEEE; 2002. p. IV-3313-IV–3316. http://ieeexplore.ieee.org/document/5745362/. Accessed 3 Apr 2024.
75. Srinidhi CL, Ciga O, Martel AL. Deep neural network models for computational histopathology: a survey. Med Image Anal. 2021;67:101813.
76. Kather JN, Calderaro J. Development of AI-based pathology biomarkers in gastrointestinal and liver cancer. Nat Rev Gastroenterol Hepatol. 2020;17:591–2.
77. Rohde GK, Ribeiro AJS, Dahl KN, Murphy RF. Deformation-based nuclear morphometry: capturing nuclear shape variation in HeLa cells. Cytometry A. 2008;73:341–50.
78. Pantic I, Cumic J, Dugalic S, Petroianu GA, Corridon PR. Gray level co-occurrence matrix and wavelet analyses reveal discrete changes in proximal tubule cell nuclei after mild acute kidney injury. Sci Rep. 2023;13:4025.
79. Alsaade FW, Aldhyani THH, Al-Adhaileh MH. Developing a recognition system for diagnosing melanoma skin lesions using artificial intelligence algorithms. Comput Math Methods Med. 2021;2021:9998379.
80. Bharathi G, Malleswaran M, Muthupriya V. Detection and diagnosis of melanoma skin cancers in dermoscopic images using pipelined internal module architecture (PIMA) method. Microsc Res Tech. 2023;86:701–13.
81. Montemarano AD, Gupta RK, Burge JR, Klein K. Insect repellents and the efficacy of sunscreens. Lancet. 1997;349:1670–1.
82. Diaz JH. Chemical and plant-based insect repellents: efficacy, safety, and toxicity. Wilderness Environ Med. 2016;27:153–63.
83. Asadollahi A, Khoobdel M, Zahraei-Ramazani A, Azarmi S, Mosawi SH. Effectiveness of plant-based repellents against different Anopheles species: a systematic review. Malar J. 2019;18:436.
84. Gu X, Kasichayanula S, Fediuk DJ, Burczynski FJ. In-vitro permeation of the insect repellent N, N-diethyl-m-toluamide (DEET) and the sunscreen oxybenzone. J Pharm Pharmacol. 2004;56:621–8.
85. Ross EA, Savage KA, Utley LJ, Tebbett IR. Insect repellent [correction of repellant] interactions: sunscreens enhance DEET (N, N-diethyl-m-toluamide) absorption. Drug Metab Dispos. 2004;32:783–5.
86. Moody RP, Wester RC, Melendres JL, Maibach HI. Dermal absorption of the phenoxy herbicide 2,4-D dimethylamine in humans: effect of DEET and anatomic site. J Toxicol Environ Health. 1992;36:241–50.
87. Hexsel CL, Bangert SD, Hebert AA, Lim HW. Current sunscreen issues: 2007 food and drug administration sunscreen labelling recommendations and combination sunscreen/insect repellent products. J Am Acad Dermatol. 2008;59:316–23.

Publisher's Note